

# Target Induced Angle Grid Regularized Estimation for Ghost Identification in Automotive Radar

Junho Kweon\* and Vishal Monga\*

\*Electrical Engineering Department, The Pennsylvania State University, University Park, PA, USA

**Abstract**—This study presents a novel algorithm for identifying ghost targets in automotive radar by estimating complex valued signal strength across a two-dimensional angle grid defined by direction-of-arrival (DOA) and direction-of-departure (DOD). In real-world driving environments, radar signals often undergo multipath propagation due to reflections from surfaces such as guardrails. These indirect paths can produce ghost targets—false detections that appear at incorrect locations—posing challenges to autonomous navigation. A recent method, the Multi-Path Iterative Adaptive Approach (MP-IAA), addresses this by jointly estimating the DOA/DOD angle grid, identifying mismatches as indicators of ghost targets. However, its effectiveness declines in low signal-to-noise ratio (SNR) settings. To enhance robustness, we introduce a physics-inspired regularizer that captures structural patterns inherent to multipath propagation. This regularizer is incorporated into the estimation cost, forming a new loss function that guides our proposed algorithm, TIGRE (Target-Induced angle-Grid Regularized Estimation). TIGRE iteratively minimizes this regularized loss and we show that our proposed regularizer asymptotically enforces  $\ell_0$  sparsity on the DOA/DOD grid. Numerical experiments demonstrate that the proposed method substantially enhances the quality of angle-grid estimation across various multipath scenarios, particularly in low SNR environments, providing a more reliable basis for subsequent ghost target identification.

## I. INTRODUCTION

Multiple-Input, Multiple-Output (MIMO) radar is useful in estimating the target information thanks to the larger degree-of-freedom coming from multiple transmitters and receivers. With this advantage, MIMO radar is used in wide range of application such as automotive radar [1], [2].

Radar can measure range, relative velocity, angle of azimuth, which can be used to understand surroundings and used for Advanced Driver Assistance Systems (ADAS). Automotive radar detect targets based on the signal received, and Direction-Of-Arrival (DOA) estimation is one of the key technique widely used in this field. While sensing surrounding environment from measured radar signals, ghost target can appear when the received signals are not directly coming from targets [3]–[5]. Specifically, multipath caused by reflections by surroundings yields ghost target whose DOA and Direction-Of-Departure (DOD) of the radar signal are different [6]. These ghost targets can burden in automotive radar operation by tracking all of actual target and ghost targets and predicting their movement [2], [3]. Therefore, for safe and robust Advanced Driver-Assistance Systems (ADAS) or autonomous driving system, it is crucial to identify ghost targets.

There have been some studies for ghost target recognition in radar. For example, the authors of [7], [8] exploit Doppler

information to detect multipath. Specifically, [7] used a linear relationship between the target and multipath ghosts once a clear range-Doppler map is acquired. However, if the target is stationary compared to the detecting automotive radar, Doppler information can be elusive. The study of [5] suggests to regard the other detected targets in very similar range are ghost targets of a target. However, this approach is not applicable when they are located in different range or can fail to detect multiple targets in similar range. The study of [4] used iterative method use the matrices whose dimensions are defined as the number of targets, so as it finds more targets, it iteratively extend the problem dimension. It is worth noting that the authors introduced the concept of group sparsity of reversibility of the first-order propagation path, which has one additional intermediate reflection compared to direct path that is the sequence of transmitter-target-receiver. However, the received signal amplitude for a first-order path and its reverse path may differ due to different phase accumulation (interference) pattern. The study of [9] proposed data-driven method that can classify ghost targets when large-scale training data with annotations is available. In synthetic aperture radar system, the authors of [10] proposed a method that can track the ghost targets back to their actual target.

The authors of [11] introduced Multi-Path IAA (MP-IAA) estimating the DOA/DOD angle grid from the received signal and identifies targets with mismatched DOA and DOD as ghost targets. MP-IAA is based on the well-known IAA algorithm for estimating DOA [12]. However, MP-IAA exhibits limited performance under low Signal-to-Noise Ratio (SNR) conditions, which are common in urban traffic scenarios.

In this paper, we develop an iterative algorithm, termed *Target Induced angle-Grid Regularized Estimation (TIGRE)*, to address DOA/DOD grid estimation. Our main contributions in this paper are outlined as follows

- **New Target Induced Regularizer:** We propose a physics-inspired regularizer that captures structural priors of ghost target inherent in multipath propagation. Specifically, we use the fact that a ghost target in the first-order path appears where either its DOA or DOD is the same with the actual target’s angular position (DOA=DOD) while the other is different.
- **Asymptotic  $\ell_0$  Sparsity in DOA=DOD Grids:** We prove that our proposed regularizer asymptotically (over the TIGRE iterations) enforces  $\ell_0$  sparsity when DOA=DOD. Such sparsity leads to more accurate ghost target estima-

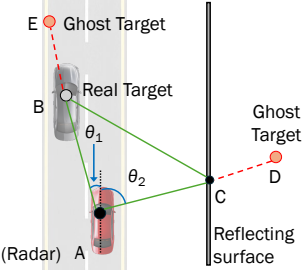


Fig. 1. Geometry of multipath propagation in automotive radar. A is the automotive radar platform, B is real target, and C is reflection point.

tion as they are induced by the actual target's presence.

- **Custom Initialization:** We propose a special initialization for TIGRE that exploits the uncertainty in the existence of ghost targets and the ambiguity in their locations. Experimentally, we validate the improvements coming from the custom initialization in both performance and enhanced convergence speed.

## II. SYSTEM MODEL

Let  $X_{g,q} \in \mathbb{C}$  is the signal magnitude and phase that is transmitted at  $q$ -th DOD and received at  $g$ -th DOA. Assuming the visible DOA/DOD are discretized into  $G$  and  $Q$  grids, we write the matrix version of  $\{X_{g,q}\}_{g=1,q=1}^{G,Q}$  as

$$\mathbf{X} = \begin{bmatrix} X_{1,1} & X_{1,2} & \cdots & X_{1,Q} \\ X_{2,1} & X_{2,2} & \cdots & X_{2,Q} \\ \vdots & \vdots & \ddots & \vdots \\ X_{G,1} & X_{G,2} & \cdots & X_{G,Q} \end{bmatrix} \in \mathbb{C}^{G \times Q}, \quad (1)$$

Let the steering vectors for transmitter and the receiver at angle  $\theta$  are  $\mathbf{a}_t(\theta) \in \mathbb{C}^{N_t \times 1}$   $\mathbf{a}_r(\theta) \in \mathbb{C}^{N_r \times 1}$ , which are

$$\begin{aligned} \mathbf{a}_t(\theta) &= \left[ 1, e^{j2\pi \frac{d_t}{\lambda} \sin \theta}, \dots, e^{j2\pi \frac{d_t}{\lambda} (N_t-1) \sin \theta} \right]^T \\ \mathbf{a}_r(\theta) &= \left[ 1, e^{j2\pi \frac{d_r}{\lambda} \sin \theta}, \dots, e^{j2\pi \frac{d_r}{\lambda} (N_r-1) \sin \theta} \right]^T. \end{aligned} \quad (2)$$

We define the steering matrices for the discretized DOD and DOA as follows:

$$\begin{aligned} \mathbf{A}_t &\triangleq [\mathbf{a}_t(\theta_{t,1}), \dots, \mathbf{a}_t(\theta_{t,G})] \in \mathbb{C}^{N_t \times G} \\ \mathbf{A}_r &\triangleq [\mathbf{a}_r(\theta_{r,1}), \dots, \mathbf{a}_r(\theta_{r,Q})] \in \mathbb{C}^{N_r \times Q}, \end{aligned} \quad (3)$$

and define the following matrix  $\mathbf{A}$ :

$$\mathbf{A} = \mathbf{A}_r \otimes \mathbf{A}_t = [\mathbf{a}_1, \mathbf{a}_2, \dots, \mathbf{a}_Q] \in \mathbb{C}^{N_t N_r \times GQ}, \quad (4)$$

where  $\otimes$  is Kronecker product and  $\mathbf{a}_i \in \mathbb{C}^{N_t N_r \times 1} \forall i$ . Using these matrices, the received signal can be expressed as

$$\mathbf{y} = \text{vec}\{\mathbf{A}_r \mathbf{X} \mathbf{A}_t^T\} + \mathbf{e} \in \mathbb{C}^{N_t N_r \times 1} = \mathbf{A} \mathbf{x} + \mathbf{e} \quad (5)$$

where  $\mathbf{x} \in \mathbb{C}^{GQ \times 1}$  is a vectorized version of  $\mathbf{X}$ , i.e.,

$$\mathbf{x} = [X_{1,1}, X_{2,1}, \dots, X_{G,1}, X_{1,2}, X_{2,2}, \dots, X_{G,Q}]^T, \quad (6)$$

and  $\mathbf{e}$  is noise.

In automotive radar, only direct paths and first-order paths are considered in general as higher-order paths naturally have

more severe path loss resulted from longer distance or can be easily distinguished by different distance comparatively [4]. The recent study of [11] proposed MP-IAA to estimate DOA/DOD angle grid to identify ghost targets. The method aims to solve the following element-wise problem:

$$\begin{aligned} \min_{X_{g,q}^n (=x_i)} f_{g,q}(X_{g,q}) &= \min_{x_i} [\mathbf{y} - x_i \mathbf{a}_i]^H \mathbf{Q}_i^{-1}(\mathbf{x}) [\mathbf{y} - x_i \mathbf{a}_i] \\ &= \min_{X_{g,q}} [\mathbf{y} - X_{g,q} \mathbf{a}_i]^H \mathbf{Q}_i^{-1}(\mathbf{x}) [\mathbf{y} - X_{g,q} \mathbf{a}_i] \end{aligned} \quad (7)$$

where  $i = g + (q-1)G$  so that  $X_{g,q} = x_i$  in (6),

$$\mathbf{a}_i = \mathbf{a}_r(\theta_{r,g}) \otimes \mathbf{a}_t(\theta_{t,q}), \quad (8)$$

and  $\mathbf{Q}_i(\mathbf{x})$  is noise covariance matrix such that

$$\mathbf{Q}_i(\mathbf{x}) = \mathbf{A} \text{diag}(|\mathbf{x}|^2) \mathbf{A}^H - x_i \mathbf{a}_i \mathbf{a}_i^H \in \mathbb{C}^{N_t N_r \times N_t N_r}. \quad (9)$$

Therefore, the problem is nonconvex where global minimum is elusive [13]. To address this minimization problem, MP-IAA updates  $X_{g,q}$  by using a closed form solution of the Weighted Least-Squares (WLS) problem in (7) with assuming  $\mathbf{Q}_i(\mathbf{x})$  is fixed and computes  $\mathbf{Q}_i(\mathbf{x})$  separately. Once correctly reconstructed from the received signal,  $X_{g,q}$  with significant amplitude ( $|X_{g,q}| \gg 0$ ) is regarded as *detected target*. The detected targets with  $\text{DOA} \neq \text{DOD}$  can be regarded as a ghost target [11].

## III. PROPOSED METHOD

### A. Target Induced Regularizer on $\text{DOA} \neq \text{DOD}$ Grids

Without losing generalizability, we set  $G = Q$  so that the diagonal elements of  $\mathbf{X}$  becomes  $\text{DOA} = \text{DOD}$  case<sup>1</sup>. From (7), we can deduce that the generalized cost to be minimized can be expressed as  $\tilde{f}(\mathbf{X}) = \sum_{g=1,q=1}^{G,Q} f_{g,q}(X_{g,q})$ . At  $n$ -th iteration step to acquire  $\mathbf{X}^{n+1}$ , we introduce the regularizer  $\mathcal{R}^n(\mathbf{X}) = \sum_{g=1,q=1}^{G,Q} \mathcal{R}_{g,q}^n(X_{g,q})$  where

$$\mathcal{R}_{g,q}^n(X_{g,q}) = \mu_{g,q}^n |X_{g,q}|^2 = \frac{1}{|X_{g,g}^n|^2 + |X_{q,q}^n|^2 + \epsilon_0} |X_{g,q}|^2, \quad (10)$$

yielding the loss function

$$\begin{aligned} \mathcal{L}^n(\mathbf{X}) &= \sum_{g=1,q=1}^{G,Q} \mathcal{L}_{g,q}^n(X_{g,q}) \\ &= \sum_{g=1,q=1}^{G,Q} f_{g,q}^n(X_{g,q}) + \lambda_{g,q} \mathcal{R}_{g,q}^n(X_{g,q}), \end{aligned} \quad (11)$$

where  $\lambda_{g,q} > 0$  controls the importance of the regularizer  $\mathcal{R}_{g,q}^n(X_{g,q}) \forall g, q, n$ .

In (10),  $\epsilon_0 > 0$  is a small positive number to prevent the denominator become zero. When either  $|X_{g,g}|^n$  or  $|X_{q,q}^n|$  is small,  $\mu_{g,q}^n > 0$  becomes large, thereby assigning greater weight to  $|X_{g,q}|^2$  in the minimization of  $\mathcal{R}_{g,q}^n(X_{g,q})$ . Therefore, this regularizer encourages that the estimated DOA/DOD

<sup>1</sup>If  $G \neq Q$ , one can still use the proposed method by applying the  $\text{DOA} = \text{DOD}$  case to the corresponding elements of  $\mathbf{X}$  in their setup.

grids  $X_{g,q}$  ( $g \neq q$ ) have a ghost target appear only when there is an actual target either  $(g, g)$  or  $(q, q)$ .

*Target Induced angle-Grid Regularized Estimation (TIGRE)* aims to solve the following element-wise (or grid-wise) loss function to acquire  $X_{g,q}^{n+1}$ :

$$\begin{aligned} X_{g,q}^{n+1} &= \arg \min_{X_{g,q}} \mathcal{L}_{g,q}^n(X_{g,q}) \\ &= \arg \min_{X_{g,q}} f_{g,q}^n(X_{g,q}) + \lambda_{g,q} \mathcal{R}_{g,q}^n(X_{g,q}) \end{aligned} \quad (12)$$

We can derive the closed form solution of (12) by differentiating  $\mathcal{L}_{g,q}^n(X_{g,q})$  with  $X_{g,q}$ :

$$\begin{aligned} \frac{\partial}{\partial X_{g,q}^*} \mathcal{L}_{g,q}^n(X_{g,q}) &= \frac{\partial}{\partial X_{g,q}^*} \{f_{g,q}^n(X_{g,q}) + \lambda_{g,q} \mathcal{R}_{g,q}^n(X_{g,q})\} \\ &= -\mathbf{a}_i^H \mathbf{W}_i^n (\mathbf{y} - X_{g,q} \mathbf{a}_i) + \frac{\lambda_{g,q} X_{g,q}}{|X_{g,q}^n|^2 + |X_{q,q}^n|^2 + \epsilon_0}, \end{aligned} \quad (13)$$

where  $\mathbf{W}_i^n = \mathbf{Q}_i^{-1}(\mathbf{x}^n)$ . Defining  $D_{g,q}^n = |X_{g,g}^n|^2 + |X_{q,q}^n|^2 + \epsilon_0$  for brevity, we can find a solution that will be in a stationary point of  $\mathcal{L}_{g,q}^n(X_{g,q})$  in terms of  $X_{g,q}$ :

$$-D_{g,q}^n \mathbf{a}_i^H \mathbf{Q}_i^{-1} (\mathbf{y} - X_{g,q} \mathbf{a}_i) + \lambda_{g,q} X_{g,q} = 0 \quad (14)$$

We can find a closed form solution of  $X_{g,q}$  as

$$X_{g,q}^{n+1} = \frac{D_{g,q}^n (\mathbf{a}_i^H \mathbf{W}_i^n \mathbf{y})}{D_{g,q}^n (\mathbf{a}_i^H \mathbf{W}_i^n \mathbf{a}_i) + \lambda_{g,q}}. \quad (15)$$

### B. Asymptotic $\ell_0$ Sparsity Behavior in DOA/DOD Grids

Regarding the effect of the proposed regularizer to the diagonal part of  $\mathbf{X}$ , we show the following lemma:

**Lemma 1.** *The proposed regularizer in (10) encourages  $\ell_0$  sparsity asymptotically in the DOA=DOD grids of  $\mathbf{X}$ , i.e., the diagonal elements of  $\mathbf{X}$  when  $G = Q$ .*

*Proof.* Let  $\mathbf{z} = \text{diag}(\mathbf{X}) \in \mathbb{C}^{G \times 1}$  and  $\tilde{\mathcal{R}}_{\text{diag}}^n(\mathbf{z}) = \sum_{g=1}^G \mathcal{R}_{g,g}^n(z_g) = \sum_{g=1}^G \mathcal{R}_{g,g}^n(X_{g,g})$ . Assuming  $z_g^n$  converges to  $\bar{z}_g$  as  $n \rightarrow \infty$ , the regularizer  $\mathcal{R}_{g,g}^n(z_g^{n+1})$  becomes

$$\lim_{n \rightarrow \infty} \mathcal{R}_{g,g}^n(z_g^{n+1}) = \lim_{z_g^n \rightarrow \bar{z}_g} \frac{|z_g^{n+1}|^2}{2|z_g^n|^2 + \epsilon_0} \quad (16)$$

As the above term is approximately  $1/2$  when  $\bar{z}_g \neq 0$  and  $0$  when  $\bar{z}_g = 0$  [14], we can approximate

$$\lim_{n \rightarrow \infty} \tilde{\mathcal{R}}_{\text{diag}}^n(\mathbf{z}^{n+1}) = \lim_{n \rightarrow \infty} \sum_{g=1}^G \mathcal{R}_{g,g}^n(z_g^{n+1}) \approx \frac{1}{2} \|\mathbf{z}\|_0, \quad (17)$$

i.e., regularizer  $\tilde{\mathcal{R}}_{\text{diag}}^n(\mathbf{z})$  is approximated as  $\ell_0$  measure of  $\mathbf{z}$ . This naturally enforces sparsity on DOA=DOD, i.e. the diagonal of  $\mathbf{X}$ . Because a  $0$  in the diagonal also encourages the corresponding row and column to be all  $0$ 's following (10) -  $\mathbf{X}$  is also expected to be sparse asymptotically.  $\square$

---

### Algorithm 1 TIGRE algorithm.

---

```

1: Inputs:  $\mathbf{y}$ ,  $G$ ,  $Q$ ,  $\epsilon_0$ ,  $\epsilon_x$ ,  $\{\lambda_{g,q}\}_{g=1,q=1}^{G,Q}$ ,  $N_{\max}$ 
2: Outputs:  $\mathbf{X}^*$ 
3: Initialize  $\mathbf{X}^0 = \text{diag}(\mathbf{x}^*)$  following (21) and (22).
4: for  $n = 0 : N_{\max}$ 
5:   Calculate  $\mathbf{Q}_i^n(\mathbf{x}^n) \forall i$  following (9) for  $\mathbf{x}^n = \text{vec}(\mathbf{X}^n)$ .
6:   Compute  $X_{g,q}^{*,n+1}$  using (15) for  $\{g, q\}_{g=1,q=1}^{G,Q}$ .
7:    $\mathbf{x}^{n+1} = \text{vec}(\mathbf{X}^{*,n+1})$ 
8:   if  $|\mathbf{x}^{n+1} - \mathbf{x}^n| < \epsilon_x$  then
9:     break
10:   end if
11: end for
12:  $\mathbf{X}^* = \mathbf{X}^{*,n+1}$ 

```

---

### C. Custom Initialization

As the existence of multipath is unknown in the beginning, we aim to find initial guess of  $\mathbf{X}$  by finding the best diagonal matrix for a given measured signal  $\mathbf{y}$ . Under this setting, the initial  $\mathbf{X}$  can be found via solving the following:

$$\min_{\mathbf{X} = \text{diag}(\mathbf{z})} \|\mathbf{y} - \text{vec}(\mathbf{A}_r \mathbf{X} \mathbf{A}_t^T)\|_2^2, \quad (18)$$

where  $\mathbf{z} = [z_1, z_2 \cdots, z_G]^T \mathbb{C}^{G \times 1}$  such that  $X_{g,g} = z_g$ .

Define the matrix  $\mathbf{C} \in \mathbb{C}^{N_t N_r \times G}$  as:

$$\mathbf{C} = [\mathbf{a}_{r,1} \otimes \mathbf{a}_{t,1}, \mathbf{a}_{r,2} \otimes \mathbf{a}_{t,2}, \cdots, \mathbf{a}_{r,G} \otimes \mathbf{a}_{t,G}], \quad (19)$$

where  $\mathbf{a}_{r,g} = \mathbf{a}_r(\theta_{r,g})$  and  $\mathbf{a}_{t,g} = \mathbf{a}_t(\theta_{t,g})$ . Then the optimization problem becomes:

$$\min_{\mathbf{z} \in \mathbb{C}^{G \times 1}} \|\mathbf{y} - \mathbf{Cz}\|_2^2 \quad (20)$$

The closed-form solution is:

$$\mathbf{z}^* = (\mathbf{C}^H \mathbf{C})^{-1} \mathbf{C}^H \mathbf{y} \quad (21)$$

Finally, the estimated diagonal matrix is:

$$\mathbf{X}^0 = \text{diag}(\mathbf{z}^*) \quad (22)$$

### D. Step-By-Step Algorithm of TIGRE

Algorithm 1 shows the step-by-step algorithm to estimate DOA/DOD angle grid  $\mathbf{X}$  from measured signal  $\mathbf{y}$ . In line 3, using the custom initialization,  $\mathbf{X}$  is initialized as  $\mathbf{X}^0$ . In line 5-7,  $\mathbf{X}$  is updated aiming to minimize the loss defined in (12) until convergence of  $\mathbf{X}$ .

## IV. NUMERICAL RESULTS

### A. Simulation Settings

We consider co-located MIMO radar with  $N_t = N_r = 8$  and  $d_t = d_r = \lambda/2$  where  $\lambda$  is wavelength. Signal-to-Noise Ratio (SNR) is set to 10 dB.  $\epsilon_x = 10^{-2}$  to decide convergence in  $\mathbf{x}$  during iteration of the competing optimization methods.

We compare TIGRE with state-of-the-art Iterative Reweighted Algorithm (IRA) [15], [16] and MP-IIA [11]<sup>2</sup>. To evaluate the performance gain of the custom

<sup>2</sup>IRA is a method for DOA estimation, but adapted to the DOA/DOD grid.

TABLE I  
DOA/DOD ANGULAR INFORMATION.

Target No.	Actual Target		Ghost 1		Ghost 2	
	$ X $	$\theta_r = \theta_t$	$ X $	$(\theta_r, \theta_t)$	$ X $	$(\theta_r, \theta_t)$
1	1	$-20^\circ$	0.7	$(-20, 40)^\circ$	0.5	$(40, -20)^\circ$
2	1	$-60^\circ$	0.7	$(-60, 60)^\circ$	0.5	$(60, -60)^\circ$
3	1	$-40^\circ$	0.7	$(-40, 50)^\circ$	0.5	$(50, -40)^\circ$

TABLE II  
AVERAGED RESULTS FOR ONE TARGET.

Method	Error ( $\downarrow$ )	Iteration ( $\downarrow$ )	Time (sec) ( $\downarrow$ )
IRA [15], [16]	4.91	<b>19.53</b>	<b>1.91</b>
MP-IAA [11]	4.58	36.59	3.25
TIGRE-no Init.	<b>3.06</b>	22.45	2.31
TIGRE	<b>0.59</b>	<b>20.07</b>	<b>2.05</b>

initialization, we simulated both TIGRE with random initialization of  $\mathbf{X}$ —marked as TIGRE-no Init.—and the custom initialization articulated in Section III-C—denoted as TIGRE. For hyperparameters of TIGRE, we set  $\lambda_{g,q} = 10$  for  $g \neq q$  and  $\lambda_{g,q} = 1$  for  $g = q$  via cross-validation [13].

### B. Simulation Results

Table II shows numerical results of the TIGRE and competing methods for single target scenario: target 1 in Table I. The values (Error  $\|\mathbf{X}^* - \mathbf{X}^{\text{true}}\|_F^2$ , number of iterations, and computational time in seconds) are average of 100 random samples for fixed target information, and the best two performance is bold faced. Both TIGRE-no Init. and TIGRE shows the smallest estimation error among the methods. TIGRE shows the second smallest number of iterations and shortest computation time, but very close to the best ones by IRA.

Table III shows the results when there are two targets: target 1 and target 2 in Table I. TIGRE shows its superiority in the estimation accuracy and the computational efficiency. The visual results shown in Fig. 2 (a), (b) are visualization of resulting DOA/DOD angle grid  $\mathbf{X}$  in this two target case, where the color denotes the value of  $|\mathbf{X}|$ . While MP-IAA and TIGRE show the best accuracy in Table III, the result of MP-IAA has multiple peaks in its diagonal part (at the location of the actual target) like  $(30, 30)^\circ$  and  $(80, 80)^\circ$ .

Table IV shows the case of three targets: target 1, 2, and 3. Again, TIGRE shows the outstanding performance among the counterparts. Fig. 2 (c), (d) show that, while MP-IAA has multiple false alarms, TIGRE produces more precisely estimated DOA/DOD angle grid. Fig. 3 shows the 1D-plot of resulting amplitude of  $\mathbf{x} (= \text{vec}(\mathbf{X}))$  and the points that is larger than 0.4 is marked. Green solid stems (with thicker line) shows true values, *i.e.*, having peaks at the three actual target locations (three peaks with the largest values) and two ghost targets of each target. Blue solid line (thinner) is the result from MP-IAA, and red dotted line is from TIGRE. While the MP-IAA yields a lot of false alarms (marked as +), TIGRE provides comparatively correct estimation (marked as  $\times$ ), especially capturing the actual targets.

In Table II-IV, the benefits of TIGRE over TIGRE-no Init. in the estimation performance and convergence speed are enabled

TABLE III  
RESULTS FOR TWO TARGETS.

Method	Error ( $\downarrow$ )	Iteration ( $\downarrow$ )	Time (sec) ( $\downarrow$ )
IRA [15], [16]	5.52	<b>14.08</b>	<b>1.26</b>
MP-IAA [11]	4.69	27.03	2.29
TIGRE-no Init.	<b>3.14</b>	17.82	1.83
TIGRE	<b>0.86</b>	<b>15.50</b>	<b>1.59</b>

TABLE IV  
RESULTS FOR THREE TARGETS.

Method	Error ( $\downarrow$ )	Iteration ( $\downarrow$ )	Time (sec) ( $\downarrow$ )
IRA [15], [16]	6.71	<b>20.68</b>	<b>1.44</b>
MP-IAA [11]	5.62	28.25	1.94
TIGRE-no Init.	<b>3.39</b>	21.58	1.54
TIGRE	<b>1.57</b>	<b>13.00</b>	<b>1.20</b>

by the custom initialization proposed in Section III-C.

### V. CONCLUSION

WE develop TIGRE - a regularized estimator over the DOA/DOD grid for ghost target identification in automotive radar. Unlike existing methods that do not consider the angular correlation between an actual target and its ghost targets, TIGRE develops target induced regularizers to mitigate the estimated signal at DOA/DOD where a ghost target cannot exist based on the estimated actual target locations. Further, custom initialization is designed that finds the best DOA/DOD estimation based on only actual targets, which is prior to ghost targets. TIGRE is shown to outperform the state of the art in both estimation accuracy and computational efficiency.

### REFERENCES

[1] J. Li and P. Stoica, *MIMO radar signal processing*. John Wiley & Sons, 2008.

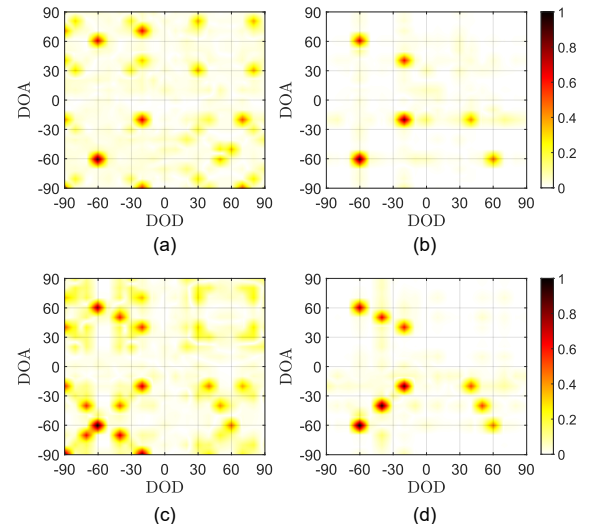


Fig. 2. Estimated DOA/DOD angle grid  $\mathbf{X}$ . (a), (b) are the case of two targets; and (c), (d) are the case of three targets. (a), (c) are from MP-IAA; and (b), (d) are from the proposed TIGRE algorithm.

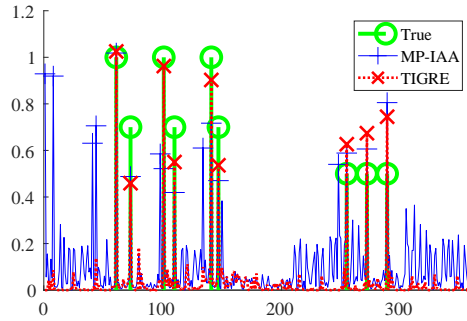


Fig. 3. Angle grids in a vector form  $\mathbf{x}$  estimated by MP-IAA and TIGRE for the scenario of three targets, each having two ghost targets.

- [2] S. Sun, A. P. Petropulu, and H. V. Poor, "Mimo radar for advanced driver-assistance systems and autonomous driving: Advantages and challenges," *IEEE Signal Processing Magazine*, vol. 37, no. 4, pp. 98–117, 2020.
- [3] D. Ammen, M. Umehira, X. Wang, S. Takeda, and H. Kuroda, "A ghost target suppression technique using interference replica for automotive fmcw radars," in *2020 IEEE Radar Conference (RadarConf20)*. IEEE, 2020, pp. 1–5.
- [4] L. Zheng, J. Long, M. Lops, F. Liu, X. Hu, and C. Zhao, "Detection of ghost targets for automotive radar in the presence of multipath," *IEEE Transactions on Signal Processing*, 2024.
- [5] C. Liu, S. Liu, C. Zhang, Y. Huang, and H. Wang, "Multipath propagation analysis and ghost target removal for fmcw automotive radars," in *IET International Radar Conference (IET IRC 2020)*, vol. 2020. IET, 2020, pp. 330–334.
- [6] I. Bilik, O. Longman, S. Villeval, and J. Tabrikian, "The rise of radar for autonomous vehicles: Signal processing solutions and future research directions," *IEEE signal processing Magazine*, vol. 36, no. 5, pp. 20–31, 2019.
- [7] R. Feng, E. De Greef, M. Rykunov, H. Sahli, S. Pollin, and A. Bourdoux, "Multipath ghost recognition for indoor mimo radar," *IEEE Transactions on Geoscience and Remote Sensing*, vol. 60, pp. 1–10, 2021.
- [8] L. B. Fertig, J. M. Baden, and J. R. Guerci, "Knowledge-aided processing for multipath exploitation radar (mer)," *IEEE Aerospace and Electronic Systems Magazine*, vol. 32, no. 10, pp. 24–36, 2017.
- [9] R. Liu, X. Song, J. Qian, S. Hao, Y. Lin, and H. Xu, "A data-driven method for indoor radar ghost recognition with environmental mapping," *IEEE Transactions on Radar Systems*, 2024.
- [10] P. Setlur, M. Amin, and F. Ahmad, "Multipath model and exploitation in through-the-wall and urban radar sensing," *IEEE Transactions on Geoscience and Remote Sensing*, vol. 49, no. 10, pp. 4021–4034, 2011.
- [11] Y. Li and X. Shang, "Multipath ghost target identification for automotive mimo radar," in *2022 IEEE 96th Vehicular Technology Conference (VTC2022-Fall)*. IEEE, 2022, pp. 1–5.
- [12] T. Yardibi, J. Li, P. Stoica, M. Xue, and A. B. Baggeroer, "Source localization and sensing: A nonparametric iterative adaptive approach based on weighted least squares," *IEEE Transactions on Aerospace and Electronic Systems*, vol. 46, no. 1, pp. 425–443, 2010.
- [13] V. Monga, *Handbook of convex optimization methods in imaging science*. Springer, 2017.
- [14] E. J. Candes, M. B. Wakin, and S. P. Boyd, "Enhancing sparsity by reweighted  $l_1$  minimization," *Journal of Fourier analysis and applications*, vol. 14, pp. 877–905, 2008.
- [15] J. Fang, F. Wang, Y. Shen, H. Li, and R. S. Blum, "Super-resolution compressed sensing for line spectral estimation: An iterative reweighted approach," *IEEE Transactions on Signal Processing*, vol. 64, no. 18, pp. 4649–4662, 2016.
- [16] W.-G. Tang, H. Jiang, and Q. Zhang, "Off-grid doa estimation with mutual coupling via block log-sum minimization and iterative gradient descent," *IEEE Wireless Communications Letters*, vol. 11, no. 2, pp. 343–347, 2021.